Materials Science and Engineering B 212 (2016) 89–95

Contents lists available at ScienceDirect

Materials Science and Engineering B

journal homepage: www.elsevier.com/locate/mseb

The influence of mechanical activation on the morphological changes of Fe/$BaTiO_3$ powder

D. Kosanović [a,*], N. Obradović [a], V.P. Pavlović [b], S. Marković [a], A. Maričić [c], G. Rasić [d,e], B. Vlahović [d,e], V.B. Pavlović [a], M.M. Ristić [f]

[a] Institute of Technical Sciences of the Serbian Academy of Sciences and Arts, Knez Mihailova 35/IV, 11000 Belgrade, Serbia
[b] Faculty of Mechanical Engineering, University of Belgrade, Belgrade, Serbia
[c] Joint Laboratory for Advanced Materials of SASA, Section for Amorphous Systems, Faculty of Technical Sciences Čačak, University of Kragujevac, 32 000 Čačak, Serbia
[d] North Carolina Central University, Durham, NC, USA
[e] NASA University Research Center for Aerospace Device Research and Education and NSF Center of Research Excellence in Science and Technology Computational Center for Fundamental and Applied Science and Education, NC, USA
[f] Serbian Academy of Sciences and Arts, Knez Mihailova 35, 11000 Belgrade, Serbia

ARTICLE INFO

Article history:
Received 21 April 2016
Received in revised form 11 July 2016
Accepted 30 July 2016
Available online 10 August 2016

Keywords:
Mechanical alloying and milling
Microstructure
Scanning electron microscopy
Raman spectroscopy
Multiferroic

ABSTRACT

Crystal structure and morphology of mechanically activated nanocrystalline Fe/$BaTiO_3$ was investigated using a combination of spectroscopic and microscopic methods. These show that mechanical activation led to the creation of new surfaces and the comminution of the initial powder particles. Prolonged milling resulted in formation of larger agglomerates of $BaTiO_3$ and bimodal particle size distribution, where $BaTiO_3$ particles were significantly larger than those of iron-containing phases. Milling times of 210 min and above lead to a significant decrease in temperature of the oxidation of iron in the sample, indicating abrupt change in reactivity. Raman spectroscopy analysis has revealed that activation had a pronounced influence on Fe/$BaTiO_3$ lattice, thereby affecting both the stability of the crystal structure and the phase transition phenomena.

© 2016 Published by Elsevier B.V.

1. Introduction

Multiferroic materials, which exhibit both electric and magnetic polarization, have recently attracted the attention of research community because of their technological applications, such as information storage and sensors, which take advantage of coupled ferroic properties [1,2]. These applications require multiferroic materials with coexistence of at least two ferroic orderings (ferroelectric, ferromagnetic or ferroelastic) [3–5]. These materials allow us to achieve efficient control of magnetization/polarization using an electric or magnetic field. However, natural multiferroic single-phase compounds are rare and none of the existing single-phase materials combines large magnetization and polarization at room temperature [6–8]. Therefore, finding new multiferroic materials with ferroic ordering and strong coupling between order parameters above room temperature is an important issue in the study of multiferroics.

Multiferroics showing strong magneto-electric coupling could lead to spin-based devices with ultralow power consumption [9–11] and novel microwave components [12]. In the case of independent switching of the ferroic ordering parameters, multiferroics could also be used in applications such as multiple-state data storage elements [13] or multifunctional photonic devices, exploiting non-reciprocal optical effects [14,15].

Smart materials, including ABO_3 ferroelectric solid solutions (like $BaTiO_3$, $SrTiO_3$, $CaTiO_3$,...), are multifunctional materials exploited in different fields of science and engineering. They feature a combination of sensors, actuators and processors. Some perovskites with ABO_3 have recently attracted attention as smart materials, i.e. as "very firm" ceramics, as substances having very large electro optic coefficients and as materials applied in the development of integrated micromechanical transistor, memory, and optical devices [16,17]. Physical properties of ABO_3 ferroelectrics strongly depend on the concentrations of their components. Based on electronic structure calculations, Xu et al. [18] predicted ferromagnetism (FM) in Fe-doped $BaTiO_3$ and have shown experimentally that 5 at.% Fe-doped $BaTiO_3$ exhibits room temperature ferro-electricity and FM with the Curie temperature (T_c) ≈ 680 K. $BaTiO_3$ is one of the materials that are being explored for multiferroicity due to its excellent ferroelectric properties such as high dielectric constant at room temperature and high ferroelec-

* Corresponding author.
E-mail address: kosanovic.darko@gmail.com (D. Kosanović).

http://dx.doi.org/10.1016/j.mseb.2016.07.016
0921-5107/© 2016 Published by Elsevier B.V.

tric transition temperature of around 400 K [19], as well as for the suitability of pyroelectric sensor application [20]. The possibility of achieving multiferroicity in $BaTiO_3$ doped with transition metals (TM) has been proposed both in experimental and theoretical studies [20,21]. Dang et al. [22,23] reported ferromagnetism in Fe- and Mn-doped $BaTiO_3$. $BaTiO_3$ has been used as a potential candidate for various applications such as capacitors, ferroelectric memories, infrared sensors, tunable microwave devices, and surface acoustic wave devices [24,25].

The aim of this study is to investigate the influence of mechanical activation on the crystal structure, microstructure and lattice dynamics of mechanically activated nanocrystalline $Fe/BaTiO_3$.

2. Materials and methods

Commercially available Fe (Aldrich, St. Louis, MO, p.a.99.99%) and $BaTiO_3$ (Aldrich, St. Louis, MO, p.a.99%) powders were mixed in 60:40 mass ratio and were mechanically activated by grinding in a planetary ball mill (Retsch PM 100) in air. Initial mixtures were ground in a zirconium-oxide container (volume 500 cm^3), together with balls of a 10 mm diameter (the ratio of the powder and the ball was 1:20). The activation time in this study was 100, 120, 150, 180, 210 and 240 min. The powder mixture were dried and calcined at a temperature of 700 °C, for 2 h inside a chamber furnace after milling.

The crystal phase of the starting powders $Fe/BaTiO_3$ (FBT) was determined by a Philips PW 1050 powder diffractogram, using $CuK\alpha_{1/2}$ filtered radiation. Tests were performed at room temperature in the range of angles 10°–90° (2θ) with a step of 0.05° and the retention time of 1 s per step. Analysis of the broadening of Bragg reflections is a very convenient way to determine the size of crystalline domains from powder diffraction data. The size of crystallites has been determined by application of Debye-Scherrer method [26]. Obtained microstructural parameters: crystallite size (D_{hkl}), density of dislocations (ρ_D) and lattice strain (e_{hkl}) are given in Tables 1 and 2.

The density of dislocations (ρ_D) was calculated through the crystallite size using following equation:

$$\rho_D = \frac{3n}{D_{hkl}^2} \quad (1)$$

n – number of dislocations on a single crystalline plane, n = 1 for random distribution of dislocations.

Microstrain was calculated using Williamson-Hall method [27]. The analysis was conducted using WINPOW Rietveld refinement framework [28].

The microstructural characterization of the mechanically activated FBT powders was performed by a Scanning Electron Microscope (SEM, JSM-6390 LV JEOL, 30 kV) coupled with EDS (Oxford Instruments X-Max^N). Before microstructure characterization, the samples were coated with gold in a sputter coater (SCD 005; BALTEC, Scotia, NY).

The average particle size (PSA), the particle size distribution, and the nature of the agglomerates in the mechanically activated FBT powders were determined using a laser particle size analyzer (Mastersizer 2000, Malvern Instruments Ltd., United Kingdom). This instrument covers the interval of particle sizes from 20 nm to 2 mm. During the measurement, the particles were dispersed in 2-propanol. For PSA measurements, powders were mixed with distilled water in an ultrasonic bath for 5 min.

The thermal stability was investigated by the differential scanning calorimetry method (DSC) using SHIMADZU DSC-50 analyzer in the temperature range from room temperature to 650 °C, with a heating rate of 20 °C/min in a nitrogen atmosphere. An amount of 25 mg of the powder was taken at the time for analysis.

The non-polarized light scattering spectra of the powder compact samples, compacted at 5 t/cm^2 (500 MPa) on a hydraulic press, were obtained at room temperature using the 633 nm line of a He-Ne laser, with a power supply of 0.6 mW at the sample. Raman scattering was recorded using a LabRam HR Evolution spectrometer (Horiba Jobin Yvon), in a backscattering geometry. The scanning range was 100–1650 cm^{-1}, with an increment step of 0.2 cm^{-1}.

Table 1
Microstructural parameters revealed by the approximation method for the $BaTiO_3$ phase of the mechanically activated samples.

Phase	D_{hkl} (nm)	ρ_D (cm^{-2})	e_{hkl} (%)
$BaTiO_3$-100	38 ± 2	0.67 ± 0.02	0.19 ± 0.01
$BaTiO_3$-120	41 ± 2	0.72 ± 0.02	0.24 ± 0.01
$BaTiO_3$-150	42 ± 2	0.89 ± 0.02	0.44 ± 0.01
$BaTiO_3$-180	36 ± 2	1.03 ± 0.02	0.51 ± 0.01
$BaTiO_3$-210	30 ± 2	1.18 ± 0.02	0.76 ± 0.01
$BaTiO_3$-240	24 ± 2	1.54 ± 0.02	0.49 ± 0.01

Table 2
Microstructural parameters revealed by the approximation method for the α-Fe phase of the mechanically activated samples.

Phase	D_{hkl} (nm)	ρ_D (cm^{-2})	e_{hkl} (%)
Fe-100	45 ± 2	0.34 ± 0.02	0.14 ± 0.01
Fe-120	42 ± 2	0.64 ± 0.02	0.18 ± 0.01
Fe-150	42 ± 2	0.65 ± 0.02	0.18 ± 0.01
Fe-180	40 ± 2	0.69 ± 0.02	0.19 ± 0.01
Fe-210	35 ± 2	0.86 ± 0.02	0.20 ± 0.01
Fe-240	30 ± 2	0.95 ± 0.02	0.22 ± 0.01

3. Results and discussion

Powder diffraction patterns of the mechanically activated mixtures (FBT-100, FBT-120, FBT-150, FBT-180, FBT-210 and FBT-240) are shown in Fig. 1. Identification of all reflections obtained was performed using the JCPDS Cards (87-0722 for Fe, 89-1428 for $BaTiO_3$, 89-7100 for FeO, 89-8104 for Fe_2O_3, 86-1356 for Fe_3O_4 and 78-0047 for ZrO_2). The presence of ZrO_2, due to sample contamination during the milling, was established primarily by other methods (results presented further in the paper), and the single line corresponding to this phase was, therefore, assigned in XRD

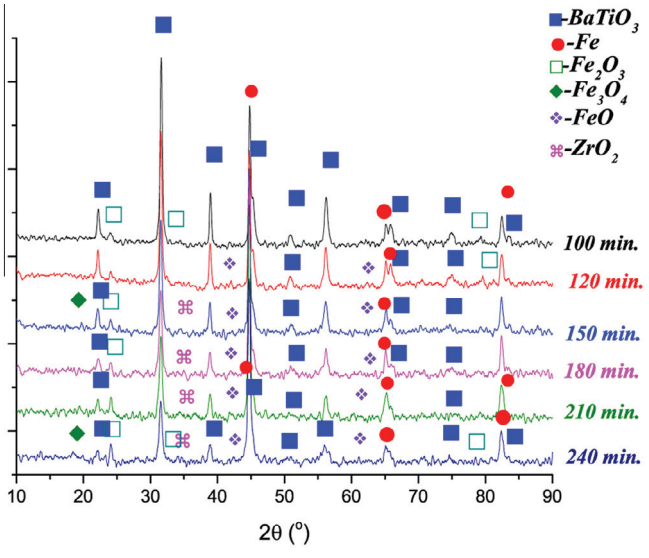

Fig. 1. Diffraction patterns of activated powders FBT.

patterns. The diffraction patterns of the sample activated for the shortest period of time (FBT-100) indicate narrow and sharp peaks of high intensity that, indicating crystalline state. After 120 and 150 min of mechanical activation, the process leads to a reduction in peak intensity and there is a change in phase composition, with the emergence of new phases FeO and Fe_3O_4, which are most likely oxidation products of iron. Based on XRD data, the following parameters were calculated: the size of the coherent scattering domains (average crystallite size, D_{hkl}), the minimum density of dislocations (ρ_D) and microstrain (e_{hkl}). These results, presented in Tables 1 and 2, show that there is no incorporation of iron into $BaTiO_3$ lattice, that the average crystallite size (D_{hkl}) for α-Fe and $BaTiO_3$ decreases with increase in activation time, while microstrain (e_{hkl}) and the minimum density dislocation (ρ_D) increase.

Fig. 2 shows the micrographs and EDS spectra of FBT samples with the magnification of 25,000. SEM micrographs of FBT-100, Fig. 2a, shows a mixture of powders forming larger agglomerates whose size is about 80 nm. It is also visible that the finer particles have twined the larger ones, as well as that the particles are spherical in shape and that they are unevenly distributed. After 120 min of mechanical activation new structures were formed (needle-shaped particles) and the samples exhibit visibly different morphology, Fig. 2b. The particles are polygonal in shape and after 120 min their size is about 50–60 nm. The micrograph of FBT-150, Fig. 2c, shows two areas: one is dominated by platelet structures of FeO, while in the other Fe-containing particles of a polygonal shape can be observed. Fig. 3 represents the SEM micrographs and EDS spectra of the FBT samples mechanically activated for 180, 210 and 240 min, with a magnification of 25,000 times. Fig. 3a and b shows that a prolonged milling time causes the rearrangement of the existing, and the formation of new phases (different iron-oxides) on the surface of particles. The process is accompanied by the agglomeration of smaller particles into larger ones, as well as incorporation of smaller particles, visible on agglomerate surface, into newly formed agglomerates. After 210 min of activation, the particles agglomerated into agglomerates between 1 and 2 μm in size.

Fig. 4 shows the particle size distribution and the cumulative distribution curve for all FBT samples. Fig. 4 shows that the FBT-100 particle size distribution consist of one fraction with two folds, i.e. two shoulders: one with the particle size of 5 μm (corresponding to $BaTiO_3$) and other of 0.5 μm (corresponding to particles of different iron-containing phases). This can be seen in Fig. 5, where green represents $BaTiO_3$ and purple represents iron-containing phases: smaller iron-containing particles are dispersed among significantly larger $BaTiO_3$ particles. After 120 min, two shoulders are more pronounced with a slight increase in the average particle size. An activation process that lasts 150 min leads to bimodal distribution with clearly defined agglomerates one originating from different iron-containing phases and the other from $BaTiO_3$. Fur-

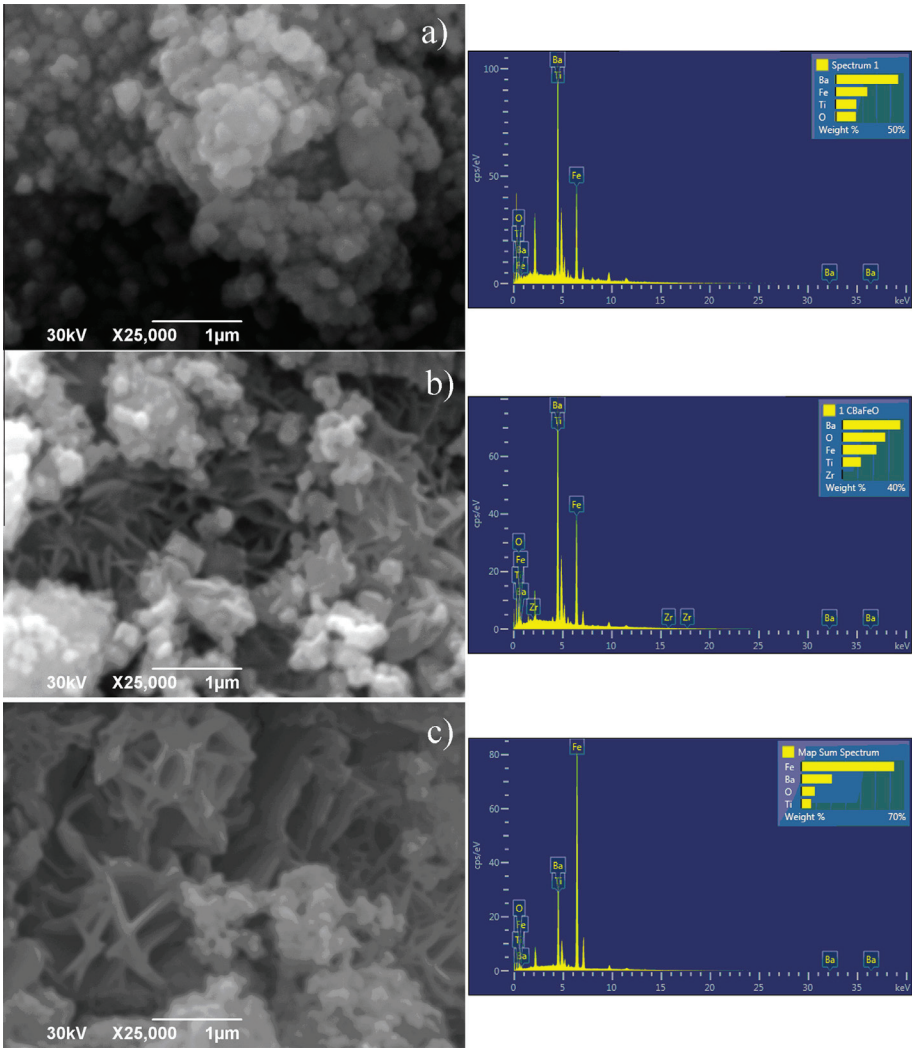

Fig. 2. SEM micrographs and EDS spectra of a) FBT-100, b) FBT-120 and c) FBT-150.

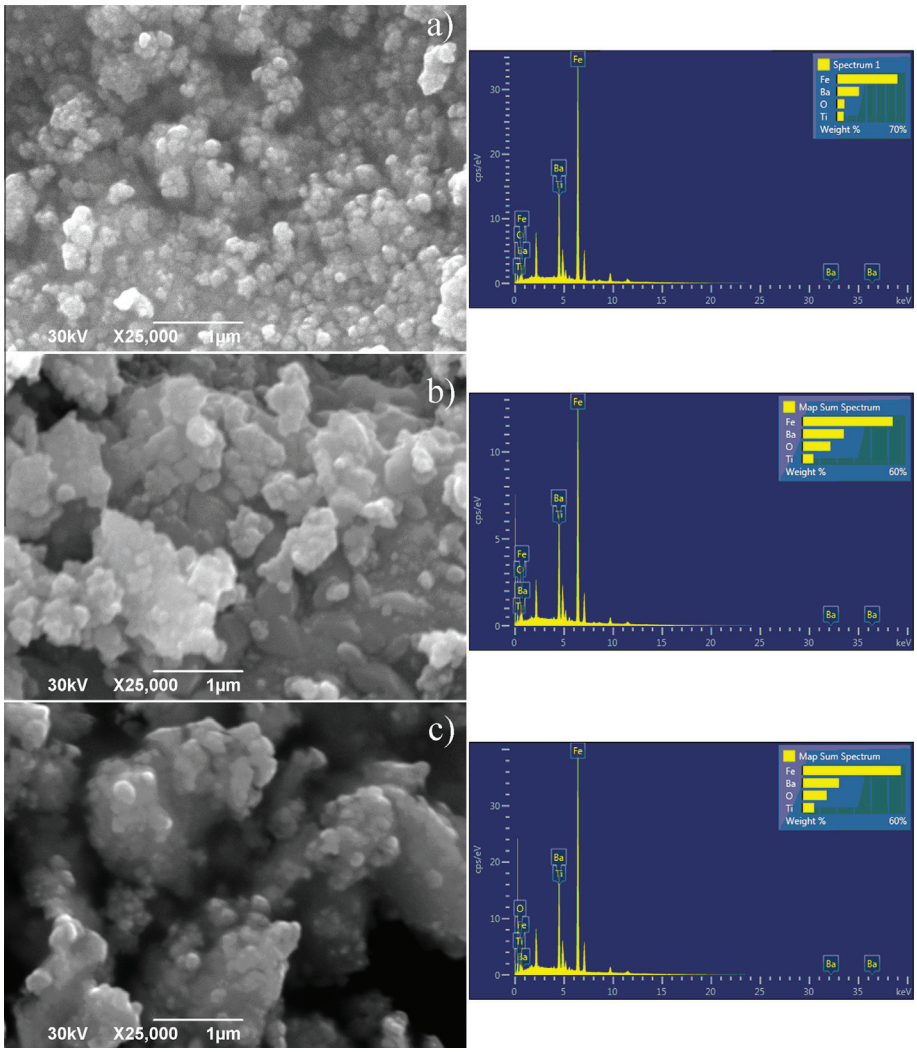

Fig. 3. SEM micrographs and EDS spectra of a) FBT-180, b) FBT-210 and c) FBT-240.

ther activation leads to an increase in particle size of agglomerates until 240 min, where narrow and more uniform distribution is observed, corresponding to recrystallization during prolonged mechanical activation.

Fig. 6 shows DSC curve for sample FBT-100. Pronounced exothermic peak is observed in all measured powders (Supplement), corresponding to the formation of three different iron-oxide phases [25]. The position of the maximum of the complex exothermic peak shifts towards lower temperatures with increased activation time. This is a common phenomenon for activated samples: when their particle size decreases, their reactivity increases, therefore less energy and lower temperature is needed for reaction.

In FBT-100 five Raman peaks corresponding to tetragonal barium titanate can be observed (Fig. 7). The number of Raman peaks in the experimental spectra of polycrystalline samples is usually smaller than the number of theoretically predicted modes, not only because of the large overlap between A_1 and E modes, and B_1 and E modes, whose frequencies in the maximum are very close to each other, but also due to the interaction of coupled modes, as well as the extreme expansion of the optical mode E with the lowest frequency (E(1TO) soft mode) [29,30]. Dominant presence of tetragonal $BaTiO_3$ structure is primarily indicated by the clearly distinct peak at 307 cm^{-1} (corresponding to the set of modes: $B_1 + E(2LO) + E(3TO)$) [31–33]. The presence of small amounts of $BaCO_3$ is also observed by weakly expressed main line of $BaCO_3$, at about 1060 cm^{-1}, which is relatively common in commercially obtained $BaTiO_3$ powders [34]. The first of the two A_{1g} modes of the hematite (crystal space group: D^6_{3d} [35]), which belongs to the strongest hematite lines, is observed as a weak line at 228 cm^{-1}, indicating that the mechanical activation of the powder led to the formation of small amount of this iron oxide phase. The second most pronounced line of the hematite (the second of five Eg modes) is not observed here, because it overlaps with a strong $A_1(2TO)$ mode of barium titanate. Therefore, only the resulting peak at ~274 cm^{-1} is recorded, which is dominated by the contribution of $BaTiO_3$ lines. With an increase in the activation time to 120 min, the decrease in the intensity and the width of the lines of the barium titanate may be observed, which is consistent with previously published results [35]. The presence of very small amounts of the Fe_3O_4 phase (spinel structure, O^7_h) and/or the FeO phase (cubic structure) is indicated by the weak line at ~665 cm^{-1}, which corresponds to the position of the strongest Raman lines in the spectra of these phases. In the samples activated for 150 min, the share of the hematite increased. This is reflected not only in the more pronounced hematite line at 225 cm^{-1} (the first A_{1g} mode [35]), but also in an increased contribution of the hematite line at ~293 cm^{-1} (the second E_g mode of the hematite [35]), which overlaps with the $BaTiO_3$ line of the A_1 (2TO) mode, causing the shift of the resulting peak from

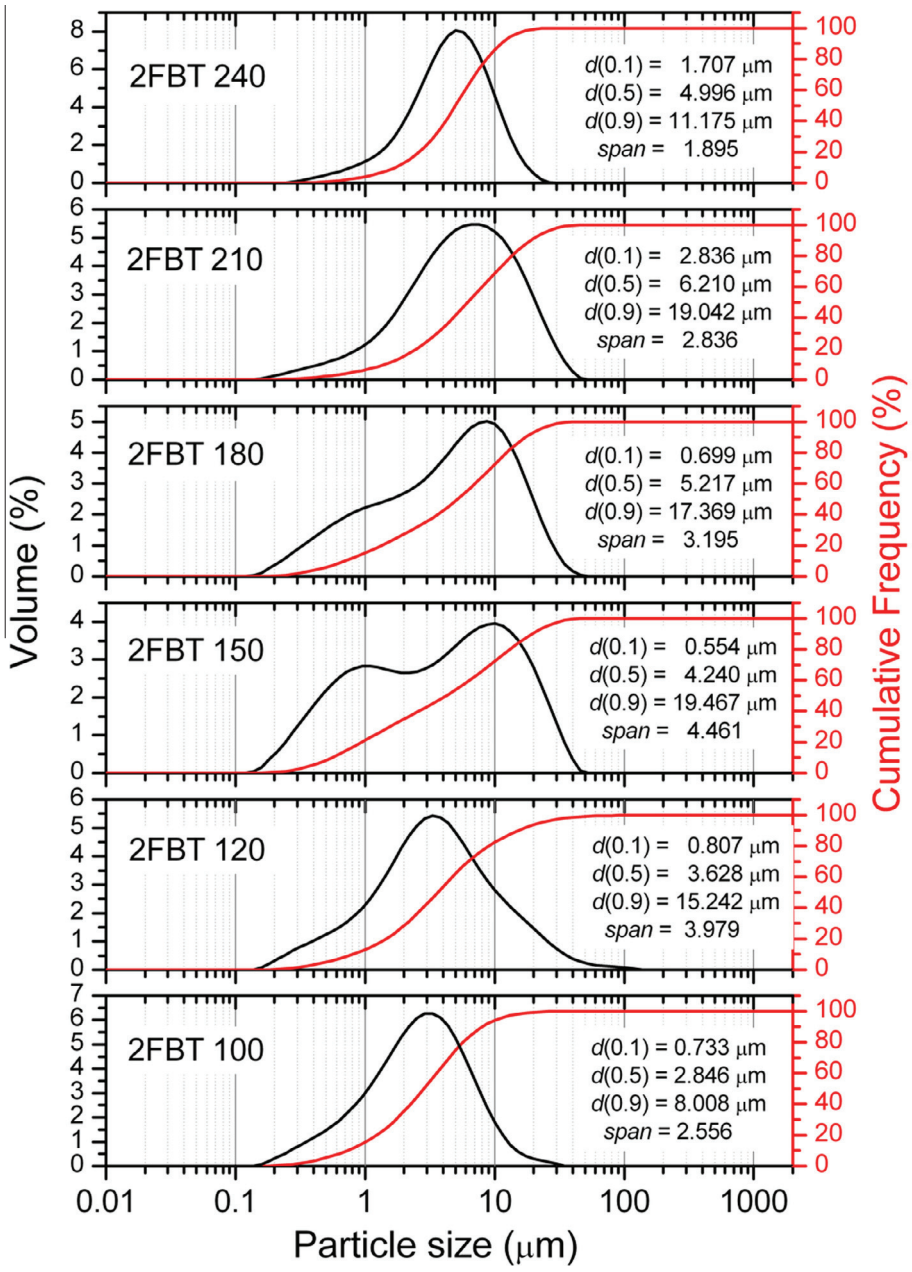

Fig. 4. Particle size distribution in the FBT powders.

~274 cm^{-1} to higher frequencies. In addition, a possible shift of the A_1 (2TO) mode to a higher frequency with increasing of the activation time ("blue shift" of the A modes in barium titanate) partly contributes to this shift, too. The occurrence of increased amount of the magnetite (Fe_3O_4) and the FeO (würstite) phase is indicated by increased intensity of lines around 665 cm^{-1}. Prolonged activation time of 180 min, leads to a further increase in intensity of the two strongest lines of the hematite, and a further decline in the intensity and the increase in the width of the $BaTiO_3$ lines. The barium titanate line at 307 cm^{-1} (characteristic for the tetragonal phase) disappears, while the wide and weak line of the barium titanate at ~715 cm^{-1}, corresponding to the A_1(3LO) + E(4LO) modes, becomes barely perceptible, because it is covered by the broad peak at ~657 cm^{-1} originating from increasingly pronounced lines of the FeO and Fe_3O_4 phases. After 240-min activation, the region between 200 and 300 cm^{-1} looks as a typical hematite spectrum: along with the three α-Fe_2O_3 lines that are present in this region (the two strongest lines of the hematite and the third one in the form of a shoulder effect), hematite lines at 400 cm^{-1} and in the 480–490 cm^{-1} region can also be observed. Moreover, a line at 615 cm^{-1} emerges in the form of a "shoulder" effect and a broad line, corresponding to the second-order scattering (the LO phonon overtone) in hematite, may be observed at 1300–1310 cm^{-1} as well [35–38]. In parallel with an increased share of hematite, the contribution of the strongest lines of FeO and Fe_3O_4 phases, at ~652 cm^{-1} and ~670 cm^{-1}, also increases. A strong line of ZrO_2, an impurity observed at longer activation times that originates from ZrO_2 containers, may also give a certain contribution to the peak within the region from 470 to 490 cm^{-1} [37]. In our study, the presence of such impurities has also been detected in the EDS and XRD analyses of powders subjected to prolonged mechanical activation. It can be observed that an increased activation time leads to the shifting of the positions of hematite and magnetite lines towards lower frequencies. For example, one of the two

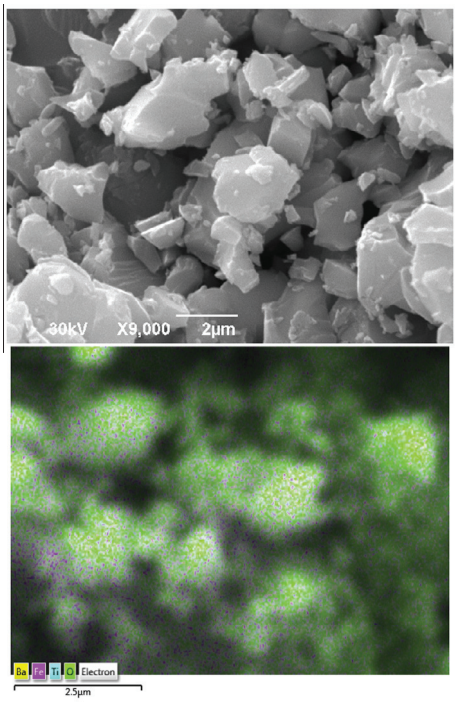

Fig. 5. Chemical mapping of FBT-100 sample showing $BaTiO_3$ particles in green and iron-containing particles in purple. (For interpretation of the references to colour in this figure legend, the reader is referred to the web version of this article.)

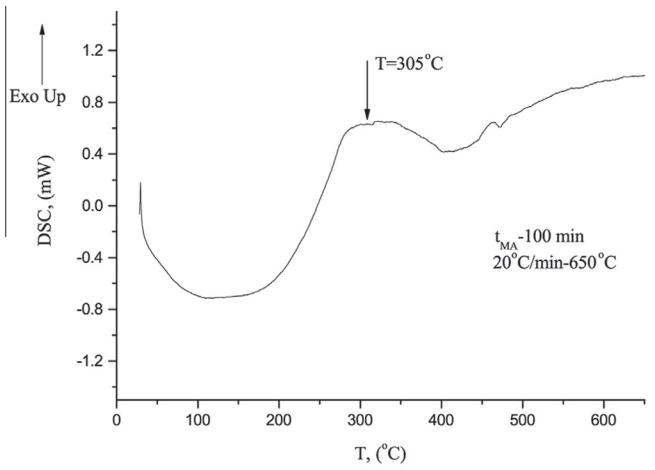

Fig. 6. DSC curve of FBT-100 sample.

strongest hematite lines of shifts from 228 cm^{-1} to 219 cm^{-1}, when the activation time is increased from 100 min to 240 min. An analogous shift of the next strongest line is not obvious for activation times up to 150 min, because that line is obscured by the stronger peak of the A_1 (2TO) mode of the barium titanate. For the activation over 150 min, this hematite line also shifts towards lower frequencies. The top of the peak originating from the contribution of the strongest line of the Fe_3O_4 and/or FeO phases also moves from 665 cm^{-1} to 652 cm^{-1} when the activation time is increased from 150 to 240 min.

4. Conclusions

In this paper, the influence of mechanical activation on the morphological changes of $Fe/BaTiO_3$ powder has been investigated. In addition, based on the diffraction patterns of powders mechanically activated for 100, 120, 150, 180, 210 and 240 min, we have obtained values for dislocation density, microstrain and the average size of crystallites of Fe and $BaTiO_3$. Based on the obtained results, we have concluded that the average crystallite size decreases with prolonged mechanical activation, while the microstrain and dislocation density increase. Microstructural investigations have shown that mechanical activation leads to the formation of new surfaces and to the comminution of the initial powder particles. The results obtained by PSA are in correlation with SEM micrographs, indicating the formation of new phases, agglomerates and recrystallization. EDS analysis and chemical mapping, combined with PSA, indicate that smaller Fe-particles are dispersed among larger $BaTiO_3$ crystals. Prolonged milling leads to incorporation of smaller iron-containing particles into larger $BaTiO_3$ agglomerates. In addition, the morphology of the powder evolves with increased milling time: needle- and polygonal-shaped crystals of different iron-containing oxide phases are formed during milling, ultimately resulting in large micron-sized agglomerates. A DSC analysis has revealed characteristic temperatures at which reactions of Fe_2O_3 phase occur. The analyses of the Raman spectra have demonstrated that the activation had a strong

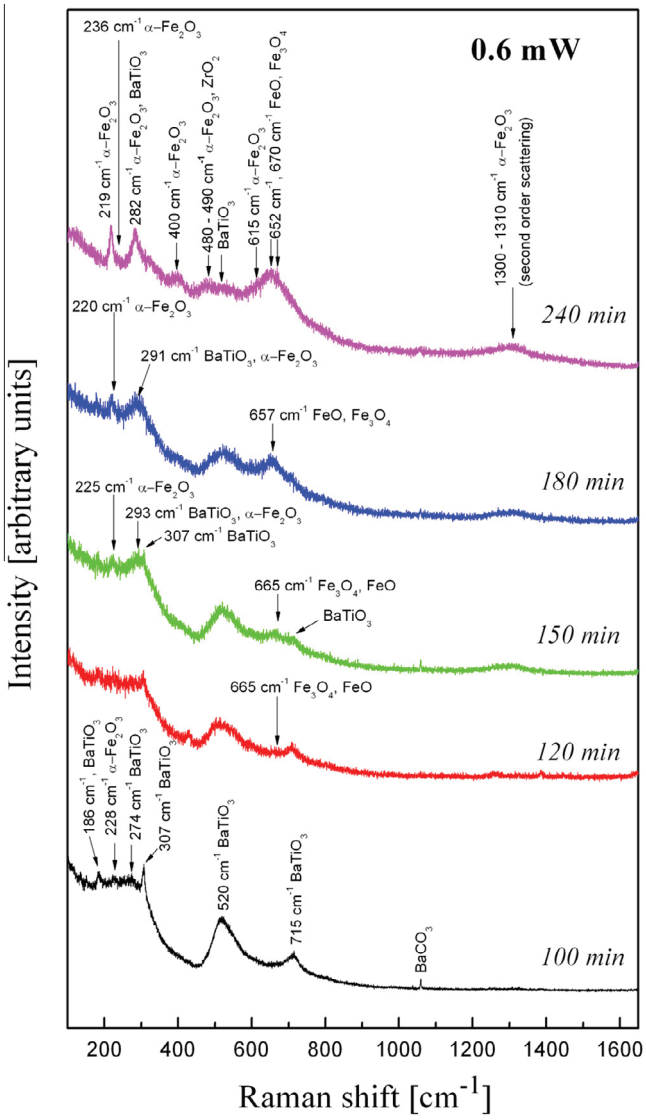

Fig. 7. Raman spectra of FBT powders.

influence on the Fe/$BaTiO_3$ lattice spectra, which affected both the stability of the crystal structure and the phase transition phenomena. Based on these results, in the further course, our research will focus on the sintering of mechanically activated systems Fe/$BaTiO_3$, as well as magnetic properties.

Acknowledgments

This research was performed within the projects OI 172057, funded by the Ministry of Education, Science and Technological Development of the Republic of Serbia and the projects F/198, funded by the Serbian Academy of Sciences and Arts. This work is also supported by the NSF (HRD-0833184), NASA (NNX09AV07A) and NSF-PREM (1523617) awards.

Appendix A. Supplementary data

Supplementary data associated with this article can be found, in the online version, at http://dx.doi.org/10.1016/j.mseb.2016.07.016.

References

[1] M. Figbig, T. Lottermoser, D. Frohlich, A.V. Golstev, R.V. Pisarev, Nature 419 (2002) 818.
[2] A.S. Džunuzović, M.M. Vijatović Petrović, B.S. Stojadinović, N.I. Ilić, J.D. Bobić, C. R. Foschini, M.A. Zaghete, B.D. Stojanović, Multiferroic (NiZn) Fe_2O_4–$BaTiO_3$ composites prepared from nanopowders by auto-combustion method, Ceram. Int. 41 (2015) 13189–13200.
[3] K.F. Wang, J.-M. Liu, Z.F. Ren, Adv. Phys. 58 (2009) 321.
[4] C.-W. Nan, M.I. Bichurin, S. Dong, D. Viehland, G. Srinivasan, J. Appl. Phys. 103 (2008) 031101.
[5] J.F. Scott, Nat. Mater. 6 (2007) 256.
[6] Z. Li, Y. Wang, Y. Lin, C. Nan, Phys. Rev. B 79 (2009) 180406.
[7] J. Wang, Y. Zhang, J. Ma, Y. Lin, C.W. Nan, J. Appl. Phys. 104 (2008) 014101.
[8] V. Berbenni, Ch. Milanese, G. Bruni, A. Girella, A. Marini, Mechanical activation of the solid-phase reaction between bismuth citrate and iron(II) oxalate dihydrate to yield $BiFeO_3$, Ceram. Int. 41 (2015) 7216–7220.
[9] C. Binek, B. Doudin, Magnetoelectronics with magnetoelectrics, J. Phys.: Condens. Matter 17 (2005) L39–L44.
[10] Y.-H. Chu et al., Electric-field control of local ferromagnetism using a magnetoelectric multiferroic, Nat. Mater. 7 (2008) 478–482.
[11] M. Bibes, A. Barthélémy, Towards a magnetoelectric memory, Nat. Mater. 7 (2008) 425–426.
[12] V.E Wood, A.E Austin, Magnetoelectric Interaction Phenomena in Crystals, in: A.J. Freeman, H. Schmid (Eds.), Gordon and Breach, 1975.
[13] M. Gajek et al., Tunnel junctions with multiferroic barriers, Nat. Mater. 6 (2007) 296–302.
[14] G.L.J.A. Rikken, E. Raupach, Observation of magneto-chiral dichroism, Nature 390 (1997) 493–494.
[15] K. Sawada, N. Nagaosa, Optical magnetoelectric effect in multiferroic materials: evidence for a Lorentz force acting on a ray of light, Phys. Rev. Lett. 95 (2005) 237402.
[16] M.E. Lines, A.M. Glass, Principles and Application of Ferroelectrics and Related Materials, Clarendon Press, Oxford, 1977.
[17] A.W. Sleight, J.L. Gillson, P.E. Bierstedt, Solid State Commun. 17 (1975) 27.
[18] B. Xu, K.B. Yin, J. Lin, Y.D. Xia, X.G. Wan, J. Yin, X.J. Bai, J. Du, Z.G. Liu, Phys. Rev. B 79 (2009) 134109.
[19] Z. Guo, L. Yang, H. Qiu, X. Zhan, J. Yin, L. Cao, Mod. Phys. Lett. 8 (26) (2012) 1250056.
[20] J. Ray, P. Hing, J. Appl. Phys. 88 (2000) 1008.
[21] H. Nakayama, H. Katayama-Yoshida, Jpn. J. Appl. Phys. 40 (2001) L1355.
[22] N.V. Dang, T.-L. Phan, T.D. Thanh, V.D. Lam, L.V. Hong, J. Appl. Phys. 111 (2012) 113913.
[23] N.V. Dang, T.D. Thanh, L.V. Hong, V.D. Lam, T.-L. Phan, J. Appl. Phys. 110 (2011) 043914.
[24] G.H. Haertling, J. Am. Ceram. Soc. 82 (4) (1999) 797–818.
[25] Z. Ristanović, A. Kalezić-Glišović, N. Mitrović, S. Đukić, D. Kosanović, A. Maričić, The influence of mechanochemical activation and thermal treatment on magnetic properties of the $BaTiO_3$–Fe_xO_y powder mixture, Sci. Sinter. 47 (1) (2015) 3–14.
[26] P. Scherrer, Göttinger Nachrichten Gesell., 2, 1918, pp. 98.
[27] G.K. Williamson, W. Hall, Acta Metall. 1 (1953) 22.
[28] K. Stahl, WINPOW Rietveld Refinement Framework, 2009.
[29] U.D. Venkateswaran, V.M. Naik, R. Naik, Phys. Rev. B 58 (1998) 14256–14260.
[30] R. Naik, J.J. Nazarko, C.S. Flattery, U.D. Venkateswaran, V.M. Naik, M.S. Mohammed, G.W. Auner, J.V. Mantese, N.W. Schubring, A.L. Micheli, A.B. Catalan, Phys. Rev. B 61 (2000) 11367–11372.
[31] W.S. Cho, E. Hamada, J. Alloys Compd. 266 (1998) 118–122.
[32] K. Suzuki, K. Kijima, J. Alloys Compd. 419 (2006) 234–242.
[33] M. El Marssi, F. Le Marrec, I.A. Lukyanchuk, M.G. Karkut, J. Appl. Phys. 94 (2003) 3307–3312.
[34] P. Duran, D. Gutierrez, J. Tartaj, M.A. Banares, C. Moure, J. Eur. Ceram. Soc. 22 (2002) 797–807.
[35] D.L.A. De Faria, S. Venaüncio Silva, M.T. de Oliveira, J. Raman Spectrosc. 28 (1997) 873–878.
[36] V.P. Pavlović, M.V. Nikolić, V.B. Pavlović, J. Blanuša, S. Stevanović, V.V. Mitić, M. Šćepanović, B. Vlahović, J. Am. Ceram. Soc. 97 (2) (2014) 601–608.
[37] Meijun Li, Zhaoci Feng, Pinliang Ying, Qin Xin, Can Li, Phys. Chem. Chem. Phys. 5 (2003) 5326–5332.
[38] M.J. Massey, U. Baier, R. Merlin, W.H. Weber, Phys. Rev. B 41 (11) (1990) 7822–7827.